INL/CON-10-18717
PREPRINT

Progress Towards Modeling of Fischer Tropsch Synthesis in a Slurry Bubble Column Reactor

American Institute of Chemical Engineers

Donna Post Guillen
Tami Grimmett
Anastasia M. Gribik
Steven P. Antal

November 2010

The INL is a
U.S. Department of Energy
National Laboratory
operated by
Battelle Energy Alliance

PROGRESS TOWARDS MODELING OF FISCHER TROPSCH SYNTHESIS IN A SLURRY BUBBLE COLUMN REACTOR

Donna Post Guillen[1], Tami Grimmett[1], Anastasia M. Gribik[1] and Steven P. Antal[2]
[1] Idaho National Laboratory Idaho Falls, Idaho, 83415 USA, Donna.Guillen@inl.gov
[2] Interphase Dynamics, Ballston Lake, NY 12019 USA, antals@rpi.edu

ABSTRACT

This paper presents a computational multiphase fluid dynamics model developed to simulate Fischer Tropsch synthesis in a slurry bubble column reactor. The work is being undertaken under the Modeling and Simulation Platform of the Idaho National Laboratory's Hybrid Energy Systems initiative to develop and demonstrate hybid energy technology. The SBCR model is one element of an integrated suite of research and development activities targeted towards our nation's pressing energy security and climate change challenges. An SBCR can be used to produce alternative fuels and value-added chemicals from syngas derived from secure domestic feedstocks, including biomass, coal, natural gas, or refuse. Although the fundamental technology was developed in the 1920s, details concerning the myriad complex processes occuring in the SBCR during FT synthesis are still not fully understood. Our team has developed a model based on a robust computational multiphase fluid dynamics platform (NPHASE-CMFD) to be used as a numerical tool or testbed for reactor optimization and design, as well as sensitivity analysis. Mechanistic submodels are connected to the main flow solver to incorporate relevant physics, such as bubble breakup/coalescence, two-phase turbulence and interfacial momentum exchange. A methodology has been developed to incorporate the dominant mechanisms of heterogeneous catalysis. Vapor-liquid equilibrium has been assimilated into the product distribution via a simple, robust property method approach. Property data is provided by a chemical process simulation package.

INTRODUCTION

The Hybrid Energy Systems Testing (HYTEST) Laboratory has been established at the Idaho National Laboratory to develop and test hybrid energy systems with the principal objective to safeguard U.S. Energy Security by reducing dependence on foreign petroleum. A central component of the HYTEST laboratory is the slurry bubble column reactor (SBCR) in which the gas-to-liquid reactions will be performed to synthesize transportation fuels using the Fischer Tropsch (FT) process. SBCRs are cylindrical vessels in which gaseous reactants (for example, synthesis gas or syngas) is sparged into a slurry of liquid reaction products and finely dispersed catalyst particles. The syngas bubbles exchange mass and momentum with the liquid phase as they react and travel though the column. The catalyst particles are transported in the slurry by the rising gas bubbles and serve to promote the chemical reaction that converts syngas to a spectrum of longer chain hydrocarbon products, which can be upgraded to gasoline, diesel or jet fuel.

In a commercial process, the gas velocity is high enough that the SBCRs operate in the churn-turbulent flow regime [1, 2] which is characterized by complex hydrodynamics, coupled with reacting flow chemistry and heat transfer, that affect reactor performance. The purpose of this work is to develop a research tool to aid in understanding the physicochemical processes occurring in the SBCR. Our team is developing a robust methodology to couple reaction kinetics and mass transfer into a four-field model (consisting of the bulk liquid, small bubbles, large bubbles and solid catalyst particles) that includes thirteen species − CO reactant, H_2 reactant, hydrocarbon product, and H_2O product in small bubbles, large bubbles, and the bulk fluid plus catalyst. Mechanistic submodels for interfacial momentum transfer in the churn-turbulent flow regime are incorporated. Bubble breakup/coalescence and two-phase turbulence submodels are also incorporated. The absorption and kinetic models, specifically changes in species

concentrations, have been incorporated into the mass continuity equation. The reaction rate is determined based on the macrokinetic model for a cobalt catalyst developed by Yates and Satterfield [3]. The model includes heat generation produced by the exothermic chemical reaction, as well as heat removal from a constant temperature heat exchanger. A property method approach is employed to incorporate vapor-liquid equilibrium (VLE) in a robust manner. Physical and thermodynamic properties as functions of changes in both pressure and temperature are obtained from VLE calculations performed external to the CMFD solver. The novelty of this approach is in its simplicity, as well as its accuracy over a specified temperature and pressure range. The focus on this paper is on the property method approach for incorporating VLE into the FT SBCR model. No CMFD results are given in this paper.

DESCRIPTION OF CMFD CODE

The computational platform for this work is the NPHASE-CMFD computer program, an unstructured, finite-volume, multifield, pressure-based computational multiphase fluid dynamics (CMFD) computer code offering both segregated and fully coupled multifield numerical solution methods. To achieve numerical convergence for multiphase flows, simulations are performed using the robust, coupled algorithm, which fully couples the phasic mass and momentum equations to solve for the phasic velocity, pressure, and volume fraction simultaneously. Although, the computer memory requirements are increased, this ability to couple the conservation of mass and momentum equations is more robust than the use of a segregated solver. A full three-dimensional, Eulerian-Eulerian framework is employed as a practical engineering tool, rather than tracking a very large number of individual bubble trajectories. Ensemble-averaged conservation equations for mass and momentum can be solved for a user-specified number of fields or phases. The conservation equations are discretized into a block matrix system, which is solved by an algebraic multigrid solver. A detailed derivation of the ensemble-averaged conservation equations has been given by Drew and Passman [4]. The fully coupled mass/momentum scheme allows any field/phase to interact with any other field/phase within the modeled system. Interfacial mass, momentum and turbulence submodels provide coupling between the fields and phases and are key to making this approach viable.

In this Eulerian-Eulerian formulation, the different phases are subdivided into one or more fields that are treated as interpenetrating continua. The probability of each field at any location is indicated by the field volume fraction. The laws of conservation of mass and momentum are satisfied for both large and small bubbles and the local velocity and volume fraction for each field are calculated at each node. The conservation of mass equation for each field-j of phase-k is expressed as

$$\frac{\partial}{\partial t}\left(\varepsilon_{jk}\rho_k\right)+\nabla\cdot\left(\varepsilon_{jk}\rho_k\underline{v}_{jk}\right)=\Gamma'''_{jk}+m'''_{jk} \tag{1}$$

where Γ'''_{jk} is the volumetric mass transfer rate due to phase change in field-j of phase-k; m'''_{jk} is the mass source of field-j from other fields of phase-k; ε_{jk} is the volume fraction of field-j of phase-k; ρ_k (kg/m^3) is the phasic density; and $\underline{v}_{jk}$ (m/s) is the velocity of field-j of phase-k. The number of fields of each phase is user-defined and allows different flow physics to be included for each field.

The ensemble-averaged, phasic momentum conservation equation can be reduced to the following approximate multifield formulation for field-j in phase-k [5]

$$\frac{\partial}{\partial t}\left(\varepsilon_{jk}\rho_k\underline{v}_{jk}\right)+\nabla\cdot\left(\varepsilon_{jk}\rho_k\underline{v}_{jk}\underline{v}_{jk}\right)=-\varepsilon_{jk}\nabla p+\nabla\cdot\varepsilon_{jk}\underline{\underline{\tau}}_k+\varepsilon_{jk}\rho_k\underline{g}+\underline{M}^i_{jk}+\Gamma'''_{jk}\underline{v}^i_{jk}+m'''_{jk}\underline{v}_{jk} \tag{2}$$

The terms on the right hand side of the equation represent the pressure gradient, shear stress tensor, body force due to gravity, momentum exchange at interfaces and momentum flux due to mass transfer. The volume fractions of the various field-j of phase-k must sum to unity

$$\sum_k \sum_j \varepsilon_{jk} = 1 \tag{3}$$

The churn-turbulent flow is modeled as a continuous liquid phase with two dispersed bubble size groups. In our four-field, ensemble-averaged CMFD model, field 1 represents the continuous liquid phase, fields 2 and 3 represent the two dispersed bubble size groups, and field 4 is the catalyst. Each bubble group is treated as a separate field to allow appropriate interfacial flow physics for the different bubble size groups to be included via the closure models. The use of mechanistic closure models for bubble forces is discussed in detail in a subsequent subsection.

For churn-turbulent flows an understanding of the expected bubble distribution is needed. Flow structure visualization studies [6] show a clear separation of bubble sizes. In reality, the bubble size distribution is polydisperse as evidenced by the experimental data [7], but since the bubble size distribution is largely bimodal, such flows may be simplified by considering the flow to consist of a small and a large bubble group. Small bubbles are spherical to ellipsoidal in shape, whereas the larger bubbles vary in size with gas flow and exhibit a distorted, spherical cap shape. A minimum of two bubble groups is needed since the interfacial forces are quite different between the groups.

The phasic energy equation implemented in NPHASE-CMFD is written as

$$\frac{\partial}{\partial t}\left(\varepsilon_{jk}\rho_k h_{jk}\right) + \nabla\cdot\left(\varepsilon_{jk}\rho_k \underline{v}_{jk} h_{jk}\right) = \nabla\cdot\left[\varepsilon_{jk}\left(\underline{\underline{q}}'' + \underline{\underline{q}}''^{T}\right)\right] + \varepsilon_{jk}\Delta H_k + UA(T_{liq} - T_w) + \Gamma'''_{jk} e^i_{jk} + m'''_{jk} e_{jk} \tag{4}$$

where h_{jk} (J/kg) is ensemble-averaged enthalpy; e_{jk} (W) is the internal energy for field-k; q"(W/m^2) is the interfacial heat flux; ΔH (W/m^3) is the chemical heat of reaction, U (W/m^2-K) is the overall heat transfer coefficient and A (m^2) is the area of the heat exchanger; and T_c and T_w are the temperatures (K) of the continuous liquid phase and the heat exchanger wall, respectively. The superscript "T" indicates the transpose of the tensor. The terms on the right hand side of the equation represent the conductive heat flux, the volumetric heat source due to the chemical reaction, and convective heat transfer to the heat exchanger, respectively. The energy equation is used to predict the change in liquid temperature due to the exothermic chemical reaction and heat exchanger. A simple heat exchanger model has been used which allows heat transfer from the liquid and represented as a constant temperature heat exchanger over the central region of the column. The heat exchanger serves to remove all of the heat of reaction (ΔH=-0.172 MJ/mol_{CO}) [1].

The local mass fractions of the chemical species are evaluated using species transport equations

$$\frac{\partial}{\partial t}\left(\varepsilon_{jk}\rho_k Y_s\right) + \nabla\cdot\left(\varepsilon_{jk}\rho_k \underline{v}_{jk} Y_s\right) = \nabla\cdot\varepsilon_{jk}\left(\frac{\mu_k}{Pr_s} + \frac{\mu_k^t}{Pr_s^t}\right)\nabla Y_s + \Gamma'''_{jk} Y_{jk} + m'''_{jk} Y_{jk} + S_s \tag{5}$$

where Y_s is the species mass fraction, μ_k and μ_k^t are the molecular and turbulent viscosity for field-k, Pr_s and Pr_s^t are the laminar and turbulent species Prandtl numbers, and S_s (kg/m^3-s) is the source term containing the reaction kinetics. It is assumed that the species are well mixed at the molecular level, that is, they have the same velocity, pressure and temperature as the carrier field.

NPHASE-CMFD includes three major sub-models to describe the following flow physics [8]: (1) bubble breakup/coalescence, (2) two-phase turbulence, and (3) interfacial momentum exchange. Bubble breakup and coalescence are important phenomena occurring in SBCRs. Small bubbles enter the flow channel and begin coalescing to form new bubbles that are twice the size of the inflow bubbles. As the

bubbles rise, the large bubbles can coalesce with either small bubbles or other large bubbles. This coalescence transitions the flow to the churn-turbulent regime. A simple, mechanistically-based breakup and coalescence model is employed [9]. Closure relations are needed to reintroduce the information that was lost as a result of averaging the conservation equations. Turbulence in the bulk fluid was modeled using a standard k-ε model with the two-phase turbulence viscosity given by Sato [10, 11]. Another set of closure models are invoked to account for the interfacial forces, which include drag, lift, wall, turbulence dispersion and virtual mass, that are included in the momentum equation. The coefficients in the interfacial momentum transfer forces can be tuned using a design optimization approach [12].

IMPLEMENTATION OF FT REACTIONS

This section describes the methodology implemented to incorporate the FT reactions into the CMFD code. The Fischer-Tropsch synthesis reaction can be modelled as a chain growth reaction of CO and hydrogen on the surface of a heterogeneous catalyst. The catalytic process converts syngas to higher molecular weight hydrocarbons where the synthetic crude carbon number distribution follows the Anderson-Schulz-Flory (ASF) distribution. This simple statistical model predicts a linear relationship between the logarithm of the molar amount of a paraffin and its carbon number. The growth probability, which fixes the slope of the ASF distribution, is catalyst dependent. The product stream is characterized by a light hydrocarbon fraction ($C_1 - C_4$), a gasoline fraction ($C_5 - C_{11}$), a diesel fraction ($C_{12} - C_{19}$) and a wax fraction (C_{20+}) as its main products, with water and carbon dioxide as by-products [13]. A cobalt catalyst was selected for the initial model since, unlike Fe catalysts, cobalt-based catalysts exhibit very little water-gas-shift (WGS) activity. Due to the minimal WGS activity, the by-product is mostly water.

To simplify the model, the FT product distribution is characterized by a representative liquid hydrocarbon (HC) product, a representative HC vapor product and water/steam. This results in modeling 13 species, which are

- CO reactant in small bubbles, large bubbles, and the bulk fluid
- H_2 reactant in small bubbles, large bubbles, and the bulk fluid
- HC wax product in small bubbles, large bubbles, and the bulk fluid, and
- H_2O product in small bubbles, large bubbles, and the bulk fluid, and
- Catalyst in bulk fluid.

The local mass fractions of the chemical species are tracked using 13 separate species transport equations. The mass fraction is tracked for the species H_2 and CO in the gas phase and HC and H_2O in the liquid and vapor phases. Absorption of gas species from both large and small bubbles into the bulk liquid phase is included. The driving force for the gas across the bubble interface into the bulk liquid will be dependent upon the interfacial species concentration in both small and large bubbles. However, because it is difficult to measure the concentration at the gas-liquid interface, coefficients for convective mass transfer across an interface for the overall driving force between the bulk concentrations in the gas and liquid phases are implemented. The product from the incorporation of absorption is the steady state concentration profile of the absorbed gas species in the bulk liquid phase and the impact of the hydrodynamics on the concentration profile.

The heterogeneous catalysis process has been simplified to model the two dominant steps: (1) absorption from the gas phase reactants into the liquid phase across the bubble interface, and (2) the chemical reaction that occurs at the catalytic sites on the catalyst surface. Other steps, such as film mass transfer, pore diffusion within the catalyst, etc. have been neglected in this model [14]. However, effects due to intraparticle diffusion and mass transfer to the catalyst surface should be investigated. Mass and heat transfer may be altered due to the resistance from the laminar layer formed around each catalyst

particle in the turbulent flow field. The resulting temperature and reactant concentrations on the catalyst surface can be much different than that in the bulk liquid.

VLE properties are computed using a chemical process simulation package (Aspen Plus from Aspen Technology, Inc.). Aspen Plus uses properties from DIPPR and other property databanks, which facilitates property validation. Using Aspen Plus, a heater block was created, which allows the temperature and pressure of the hydrocarbon stream exiting the FT reactor to be varied. The hydrocarbon product stream is then sent to a flash drum where it is separated into vapor and liquid streams (Figure 1). A sensitivity operation is used to calculate the various thermodynamic and physical properties for the liquid and vapor streams, as well as the vapor fraction exiting the heater block. The Peng-Robinson thermodynamics package is used. Then, based on the temperature and pressure, the appropriate split between liquid and vapor products can be calculated and the associated properties using the equations regressed from the data. Depending upon the temperature and pressure of the operating column, H_2O may experience a phase change and both liquid and vapor are present. A list of physical and thermodynamic properties needed for the hydrocarbon and water liquid and vapor, and for the hydrogen and carbon dioxide vapor, is given in Table 2.

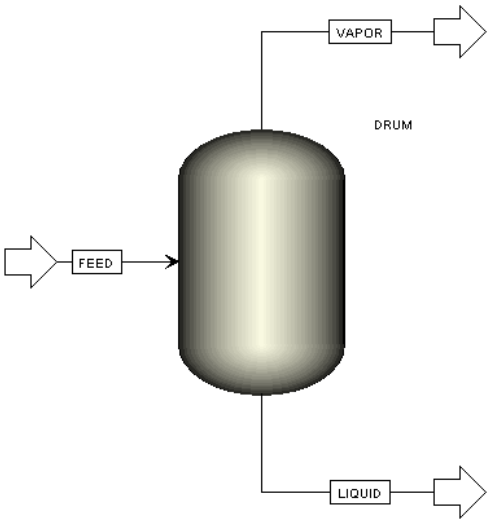

Figure 1. Illustration of flash drum used to separate liquid and vapor components in Aspen Plus.

This methodology provides reactant and product properties that are functions of reactor temperature and pressure. The expressions have the general form

$$\phi(T,P) = \xi_1 TP + \xi_2 P^2 + \xi_3 P + \xi_4 + \xi_5 T + \xi_6 T^2 \tag{6}$$

where $\phi(T,P)$ represents a physical quantity (such as molecular weight, density, viscosity, etc.) listed in the left column of Table 1. All physical properties are calculated based on temperature and pressure of the current computational cell. All properties are in SI units, pressure is in Pa and temperature is in K for all equations listed, unless otherwise noted. The property equations derived by regression from the Aspen Plus simulation results are valid over a temperature range from 423 to 623 K and a pressure range from 2.4 to 3.4 MPa. The regression coefficients are tabulated in the Appendix.

Table 1. Physical and thermodynamic properties specified for the FT reactants and products (L=liquid; v=vapor).

	HC	H_20	H_2	CO
heat capacity, c_p (J/kmol-K)	L,v	L,v	v	v
thermal conductivity, k (W/m-K)	L,v	L,v	v	v
molecular weight , MW (kg/mole)	L,v	L,v	v	v
Prandtl number, Pr (-)	L,v	L,v	v	v
density, ρ (kg/m^3)	L,v	L,v	v	v
viscosity, μ ($N-s/m^2$)	L,v	L,v	v	v
surface tension, σ (N/m)	L	L	N/A	N/A
diffusivity in HC phase, D (m^2/s)	N/A	N/A	v	v
Henry's constant, H (-)	N/A	N/A	v	v
volume fraction, ε (-)	v	v	N/A	N/A

The trick to making the property method approach work with the CMFD code is to stabilize the solution by referencing the hydrodynamic pressure. If the local system pressure is used for the properties, initial instabilities in the calculation as convergence is approached are amplified causing the CMFD simulation to diverge. For this reason, the hydrodynamic pressure (a function of column height) is used in the equations for the various reactant and product properties. As shown in the energy equation, the CMFD code uses enthalpy, rather than temperature. A subroutine to derive local temperature from enthalpy and specific heat was written, since the property expressions use temperature whereas the CFMD code uses enthalpy. Expressions for the properties are then connected to the main NPHASE-CMFD solver via user-defined subroutines. This approach allows the incorporation of VLE without all the added baggage of doing complex, time-consuming calculations within the CMFD code.

The procedure employed by the property-method approach is described in detail below and depicted in Figure 2. The VLE simulation performed in Aspen is used to obtain equations for the various physical and thermodynamic properties and parameters. The CMFD solution is initialized with a set of initial conditions. The initial temperature and pressure are provided to the routines indicated by "FT reactions." The results of these routines includes: (1) properties, (2) the mass transfer source term, and (3) the species source term, which are used by the CMFD code. The CMFD results are checked for convergence. If the solution has converged within an acceptable residual, the spatial distribution of velocity, temperature, pressure, phase hold-up and species within the SBCR are output. If not, the updated temperature and pressure are used in the "FT reactions" routines and the CMFD code iterates until convergence within a specified tolerance is achieved.

Step 1: Calculate properties for liquid hydrocarbon

First, determine the physical properties of the bulk liquid hydrocarbon using equation coefficients (ξ_1 through ξ_6) listed in Table A1.

Step 2: Calculate properties of gas bubble mixture

Gas mixture properties are calculated by the mixture rule

$$\phi_{mix,k}(T,P) = \sum_s \phi_{s,k}(T,P) Y_{s,k} \tag{7}$$

where the terms are summed over the number of gaseous species, s. The mass fraction, Y_s, is related to the molar concentration c_s (moles/m^3) of species s by

$$Y_s = \frac{MW_s c_s}{\rho_k} \tag{8}$$

where MW_s (kg/mole) is the molecular weight for species, s. The physical properties of the bubbles are determined using Equation 6 with the equation coefficients listed in Tables A2 and A3. For example,

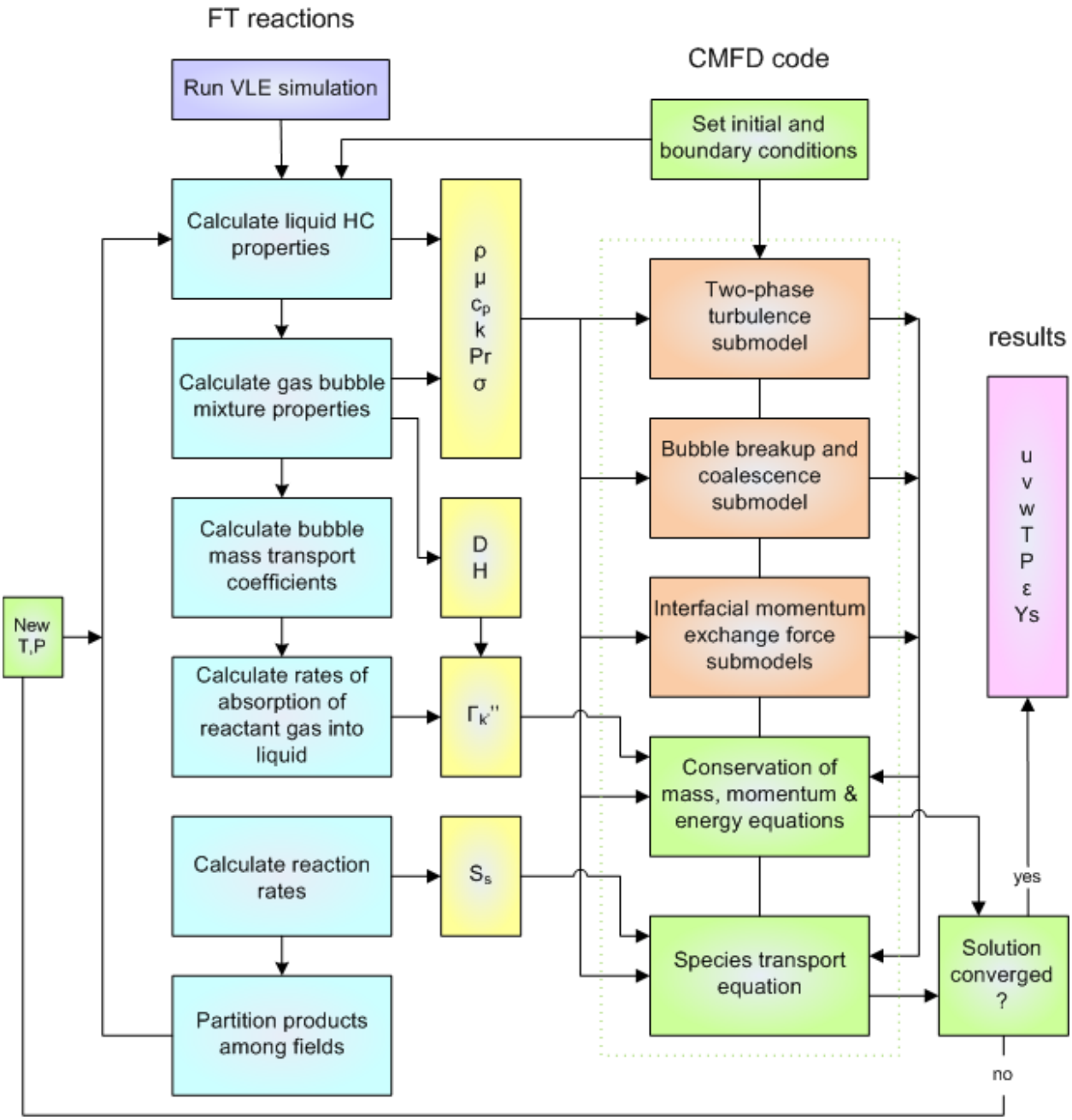

Figure 2. Incorporation of property method approach into solution methodology.

to calculate the initial mixture properties of the gas in the bubbles, multiply the pure CO and H_2 physical properties by their corresponding mass fraction and sum. For a gas mixture comprised of only CO and H_2, the expression for the small bubble (sb) field is

$$\phi_{mix,sb}(T,P) = \phi_{CO,sb}(T,P)Y_{CO,sb} + \phi_{H2,sb}(T,P)Y_{H2,sb} \tag{9}$$

and, similarly, for the large bubble (lb) field

$$\phi_{mix,lb}(T,P) = \phi_{CO,lb}(T,P)Y_{CO,lb} + \phi_{H2,lb}(T,P)Y_{H2,lb} \tag{10}$$

where density, viscosity, specific heat, thermal conductivity and Prandtl number are substituted for the variable ϕ. Once the syngas has reacted and gaseous hydrocarbon products and water vapor are produced, these additional components must be included in the mixture property calculation.

Step 3: Calculate small and large bubble mass transport coefficients

After the initial physical properties are calculated for the wax and bubble mixtures, the mass transport rates and reaction rates are calculated as described in [14]. The mass transfer coefficient for large and small bubbles for each gas species is calculated based on the diffusion coefficients regressed from the Aspen Plus output. First, the diffusion coefficient is calculated for CO and H_2 in the liquid hydrocarbon (wax) product, using the coefficient data for CO and H_2 given in Table A4.

Then, the volumetric mass transport coefficient for CO and H_2 in small and large bubbles is calculated as a function of gas holdup and diffusivity [1]

$$\frac{k_L a_{s,sb}}{\varepsilon_{sb}} = 1.0\sqrt{\frac{D_{L,s}}{D_{L,ref}}} \tag{11}$$

$$\frac{k_L a_{s,lb}}{\varepsilon_{lb}} = 0.5\sqrt{\frac{D_{L,s}}{D_{L,ref}}} \tag{12}$$

where $k_L a_s$ (s^{-1}) is the overall mass transfer coefficient for species s, ε_{lb} and ε_{sb} are the gas holdup for large bubbles and small bubbles (calculated by NPHASE), $D_{L,s}$ (m^2/s) is the diffusivity for species s in the liquid phase, and $D_{L,ref}$ (m^2/s) is the reference diffusion coefficient [1] in the liquid (2×10^{-9} m^2/s).

Step 4: Calculate rates of absorption of reactant gas to bulk liquid phase

Next, the rate of absorption is calculated for CO and H_2 from the large bubbles and small bubbles, using the mass transfer coefficient calculated above and the equilibrium gas concentration in the liquid phase, based on the Henry's law constant. The Henry's law constant, H_s, is calculated from the data listed in Table A5.

The following equation describes the rate of mass transfer ($\Gamma'''_{s,k}$, mol/m^3-s) for the solute (gas) into the solvent (liquid):

$$\Gamma'''_{s,k} = k_L a_{s,k} \left(c_s^* - c_{s,L} \right) \tag{13}$$

where

$$c_s^* = \frac{c_{s,v}}{H_s} \tag{14}$$

1. where c_s^* is the equilibrium concentration of species s in the gas phase with the liquid (mol/m^3), $c_{s,L}$ is the current concentration of species s in the liquid phase (mol/m^3), $c_{s,v}$ is the current concentration of species s in the gas phase (mol/m^3), and H_s is the Henry's law constant for species s, calculated above. Figure 3 depicts the concentration profiles at the gas bubble-bulk liquid interface. The diffusion coefficient controls the rate of mass transfer of gases into the bulk liquid, whereas the solubility determines the amount of gas that will dissolve eventually in the liquid phase. Film mass transfer (bulk diffusion) of the products from the external surface of the solid catalyst particle through the boundary layer has been neglected.

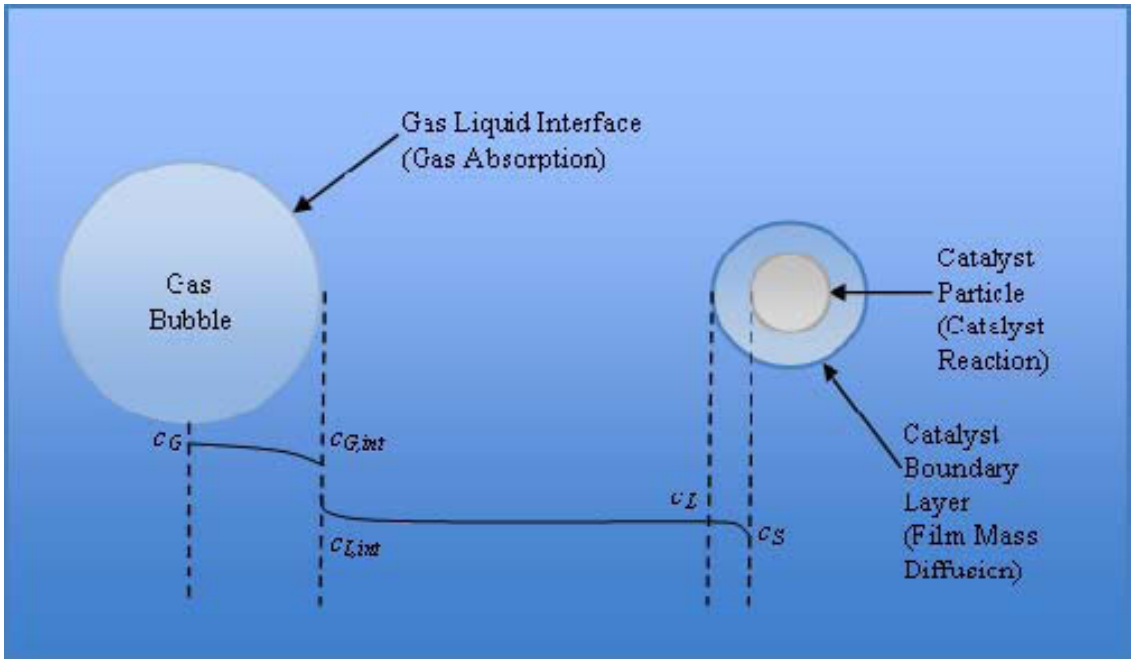

Figure 3. Concentration profile in the SBCR.

Rates of absorption are calculated for CO and H_2 from large and small bubbles, using the above method. Using these calculated rates of absorption, the resulting concentration of CO and H_2 in the bulk liquid is calculated in NPHASE-CMFD. This concentration of CO and H_2 will then be used in the reaction rate expressions given below. By combining the four equations listed above, the source terms for the conservation equations are obtained. The rates of absorption for the small bubbles is expressed as

$$\Gamma'''_{CO,sb} = 1.0 \sqrt{\frac{D_{L,CO}}{D_{L,ref}}} \left(\left(\frac{c_{CO,v}}{H_{CO}} \right) - c_{CO,L} \right) \varepsilon_{sb} \tag{15}$$

$$\Gamma'''_{H2,sb} = 1.0\sqrt{\frac{D_{L,CO}}{D_{L,ref}}}\left(\left(\frac{c_{H2,v}}{H_{H2}}\right) - c_{H2,L}\right)\varepsilon_{sb} \tag{16}$$

and the rates of absorption for the large bubbles is expressed as

$$\Gamma'''_{CO,lb} = 0.5\sqrt{\frac{D_{L,CO}}{D_{L,ref}}}\left(\left(\frac{c_{CO,v}}{H_{CO}}\right) - c_{CO,L}\right)\varepsilon_{lb} \tag{17}$$

$$\Gamma'''_{H2,lb} = 0.5\sqrt{\frac{D_{L,H2}}{D_{L,ref}}}\left(\left(\frac{c_{H2,v}}{H_{H2}}\right) - c_{H2,L}\right)\varepsilon_{lb} \tag{18}$$

In the CMFD code, Γ''' are the source terms for the ensemble-averaged phasic mass transfer rate.

Step 5: Calculate reaction rates

To determine the consumption of CO and H_2 for the FT reaction, it is necessary to calculate the molecules of carbon and hydrogen required to form the product to ensure that enough CO and H_2 have absorbed into the wax phase and reacted on the catalyst surface for the reaction to proceed. This is a limitation of modeling the kinetics macrokinetically. Unfortunately, a microkinetic model of sufficient rigor does not currently exist for FT catalysts, so we are limited to a macrokinetic approach [13]. It is assumed that the catalyst particles are sufficiently small such that external and internal mass and heat transfer are not rate limiting. The intrinsic kinetic expression for the consumption of CO and H_2, which is a Langmuir-Hinshelwood type expression, was based on data collected over a range of industrially relevant conditions. A macrokinetic approach using power rate laws is used, where the heterogeneous catalytic reaction is expressed in terms of the rate of consumption of CO as [3]

$$R_{CO} = \frac{-a c_{CO,L} c_{H_2,L}}{\left(1 + b c_{CO,L}\right)^2} \tag{19}$$

with the kinetic constant, a $\left(\frac{m^6}{kg_{cat}\,s\,mol}\right)$, and the adsorption coefficient, b $\left(\frac{m^3}{mol}\right)$, defined as follows

$$a = 8.852 \times 10^{-13}\ \exp\left[4494.41\frac{1}{K}\left(\frac{1}{493.15} - \frac{1}{T}\right)\right]\left(R_{gas}\,T\right)^2 \tag{20}$$

$$b = 2.226 \times 10^{-5}\ \exp\left[-8236.15\frac{1}{K}\left(\frac{1}{493.15} - \frac{1}{T}\right)\right]R_{gas}\,T \tag{21}$$

where R_{CO}, R_{H2}, R_{H2O}, and R_{HC} (mol/kg_{cat}s) are the rates of consumption for CO and H_2 and the rate of production for H_2O and HC, respectively, R_{gas} (J/mol-K) is the gas constant, and T (K) is the temperature of the catalyst.

To determine the number of moles of hydrogen and carbon in the product, it is assumed that the hydrocarbon product is a C_nH_{2n+2} (paraffin) molecule. Based on this calculation, the appropriate rate of hydrogen consumption, hydrocarbon production, and water production can be implemented. For instance, if the current temperature and pressure is 493.15K and 2930271.85 Pa, the volume fraction in the

hydrocarbon product is approximately 0.9700. The molecular weight of the liquid is ~280.15 g/mol and the molecular weight of the vapor is 24.47 g/mol. As a result the average molecular weight is

$$MW_{avg} = 0.97 \cdot 24.47 \frac{g}{mol} + (1 - 0.97) \cdot 280.15 \frac{g}{mol} = 32.14 \frac{g}{mol} \tag{22}$$

based on the chemical formula $C_nH_{(2n+2),}$ if the molecular weight of carbon is 12.011 g/mol and the molecular weight of hydrogen is 1.00794 g/mol, n is equal to 2.15

$$32.14 \frac{g}{mol} = 12.011 \cdot n + 1.00794 \cdot (2n + 2) \rightarrow n = 2.15 \tag{23}$$

and if the chemical reaction formula for the production of alkanes is as follows [15]

$$nCO + (2n + 1)H_2 \rightarrow C_nH_{(2n+2)} + nH_2O \tag{24}$$

the rates of consumption and formation of H_2, H_2O, and hydrocarbon product are

$$R_{H_2} = \left(\frac{2n + 1}{n} \right) (R_{CO}) \tag{25}$$

$$R_{H_2O} = -(R_{CO}) \tag{26}$$

$$R_{HC} = -\frac{1}{n} (R_{CO}) \tag{27}$$

To obtain reaction rate in units of rate of change of moles per volume $\left(\frac{mol}{m^3 s} \right)$, the reaction rates are multiplied by the density of the catalyst and the corresponding catalyst volume fraction. The species source term due to chemical reactions is summed from the contributions of the reaction rates

$$S_s = MW_s \sum_{n=1}^{N_R} n_{sn} R_n \tag{28}$$

where MW_s is the molecular weight (kg/mol) for species *s*, n_{sn} is the overall stoichiometric coefficient for species *s* in reaction *n* (positive for products and negative for reactants), N_R is the number of reactions and R_n is the reaction rate for the n^{th} reaction. The species source term is fed into the species transport equation.

Step 6: Partition products among fields

After the rates of formation are determined, the products formed must be partitioned to either the liquid or vapor phase. Therefore, the moles of hydrocarbon product formed are partitioned to the liquid wax phase by multiplying the moles formed by one minus the vapor fraction. The moles of vapor product are the vapor fraction times the moles formed. The vapor product is assumed to be equally divided amongst the various bubble sizes. It should be noted that the coefficients of the reaction expressions, i.e. how many moles of CO and H_2 are reacted are dependent upon the number of CO and H_2 molecules formed in the reaction product. To determine this, the volume fraction of the hydrocarbon product is calculated, based on the current temperature and pressure. The molecular weight of the hydrocarbon mixture is then calculated using the corresponding volume fraction of liquid and vapor using the

equations for the vapor and liquid molecular weights. The coefficients in the regressed equations for volume fraction, ε, and molecular weights, MW, of the hydrocarbon product are given in Table A6.

$$MW_{HC,mix} = \varepsilon_{HC} MW_{HC,v} + (1 - \varepsilon_{HC}) MW_{HC,L} \tag{29}$$

The water product formed is then determined to be either a liquid or vapor product. This is accomplished by inputting the current temperature into equation for pressure. The coefficients of this pressure equation are given in Table A7. The regressed equation for water partial pressure is

$$P_{H2O}(T) = \xi_7 T^3 + \xi_8 T^2 + \xi_9 T + \xi_{10} \tag{30}$$

If the calculated pressure is less than the current system pressure, the water formed is a liquid product and joins the wax phase, if the pressure is greater than or equal to the current pressure the water is in the vapor phase and should be partitioned equally amongst the various bubble sizes.

Step 7: Calculation of gas mixture properties

The resulting properties of the gas phase for all bubble sizes and the liquid phase are calculated using general mixture rules for the next computational node according to steps one and two above. The mixture rule given is used to obtain the properties of the gaseous and liquid mixtures. However, the gas mixture now must include the gaseous properties of the hydrocarbon product formed, and depending on which phase it is present in, either the liquid or gas phases must include the water mixture properties. Coefficients for the property equations are given in Tables A8 through A10.

Step 8: Repeat Steps 3 through 7 above

Steps three through seven described above are repeated with updated temperatures and pressures from the CMFD solution. This procedure continues until convergence of the CMFD simulation has been achieved.

SUMMARY AND FUTURE WORK

A CMFD model developed for simulation of FT reactions in a SBCR has been presented. A four-field, 13-species model was created to predict churn-turbulent flows in a SBCR. The churn-turbulent flow is modeled as a continuous liquid phase with two dispersed bubble size groups using an Eulerian-Eulerian framework. Each bubble group is treated as a separate field to allow appropriate flow physics for the different bubble size groups to be included via the closure models. The use of mechanistic closure models accounts for interfacial momentum transfer between the bubbles and the liquid wax. Bubble breakup/coalescence and two-phase turbulence submodels are incorporated into the NPHASE-CMFD code. A property method approach to incorporating VLE into the calculation is outlined. An Aspen Plus simulation was executed and the resulting data was regressed into a set of equations for the physical and thermodynamic properties that are functions of reactor temperature and pressure. This approach allows the incorporation of VLE without all the complexity of performing time-consuming calculations within the CMFD code.

Physical processes that have been neglected here for the purpose of simplification should be investigated to determine their effect. Specifically, diffusion across the boundary layer near the catalyst surface may affect the heat and mass transfer. Future work to improve on the current model includes obtaining an expression for the ASF product distribution as a function of temperature and pressure. A more detailed model of the heat exchanger tubes within the SBCR, including the pressure drop and other flow effects due to the presence of internals, should be included. Most importantly, validation of the

simulation results will be necessary using data from an operating SBCR. Results from the SBCR model will be presented after the validation has been performed.

ACKNOWLEDGMENTS

Funding for this research was supported by the U.S. Department of Energy, Office of Nuclear Energy, under DOE Idaho Operations Office Contract DE-AC07-05ID14517.

REFERENCES

1. Maretto, C. and R. Krishna, *Modelling of a bubble column slurry reactor for Fischer-Tropsch synthesis.* Catalysis Today, 1999. **52**(2-3): p. 279-289.
2. Fernandes, F.A.N., *Modeling and Product Grade Optimization of Fischer-Tropsch Synthesis in a Slurry Reactor.* Ind. Eng. Chem. Res. , 2006. **45**: p. p. 1047-1057.
3. Yates, I.C. and C.N. Satterfield, *Intrinsic Kinetics of the Fischer-Tropsch Synthesis on a Cobalt Catalyst.* Energy & Fuels, 1991. **5**: p. 168-173.
4. Drew, D.A., Passman, S.L.. *Theory of Multicomponent Fluids.* Applied Mathematical Sciences, 1998. **Vol. 135**.
5. Podowski, M.Z., *On the Consistency of Mechanistic Multidimensional Modeling of Gas/Liquid Two-Phase Flows.* Nucl. Eng. Des. , 2009. **doi:10.1016/j.nucengdes.2008.10.022**.
6. Lopez de Bertodano, M., Sun, X., Ishii, M., Ulke, A., *Phase Distribution in the Cap Bubble Regime in a Duct.* Journal of Fluids Engineering, 2006. **Vol. 128**: p. p. 811-818.
7. Lucas, D., Beyer, M., Kussin, J., Schutz, *Benchmark Database on the Evolution of Two-Phase Flows in a Vertical Pipe*, in *XCFD4NRS, OECD/NEA & International Atomic Energy Agency (IAEA) Workshop*. 2008: Grenoble, France.
8. Guillen, D.P., et al., *Development of a Computational Multiphase Flow Model for Fischer Tropsch Synthesis in a Slurry Bubble Column Reactor*, in *XIX International Conference on Chemical Reactors, CHEMREACTOR-19* 2010: Vienna, Austria.
9. Antal, S.P., M.Z. Podowski, R.T. Lahey, Jr., D. Barber, C. Delfino, *Multidimensional Modeling of Developing Two-Phase Flows in a Large Adiabatic Riser Channel*, in *The 11th International Topical Meeting on Nuclear Reactor Thermal-Hydraulic (NURETH-11)*. 2005: Popes Palace Conference Center, Avignon, France.
10. Sato, Y., Sekoguchi, K., *Liquid Velocity Distribution in Two-Phase Bubble Flow.* Int. J. Multiphase Flow, 1975. **Vol 2**: p. 79-95.
11. Sato, Y. and M. Sadatomi, *Momentum and Heat Transfer in Two-Phase Bubble Flow - I.* International Journal of Multiphase Flow, 1981. **7**(2): p. 167-177.
12. Guillen, D.P., et al., *Optimization of a Two-Fluid Hydrodynamic Model of Churn Turbulent Flows*, in *Proceedings of the 17th International Conference on Nuclear Engineering, ICONE17-75113*. 2009: Brussels, Belgium.
13. Bartholomew, C.H., Farrauto, R.J., *Fundamentals of Industrial Catalytic Processes*. Second Edition ed. 2006, Hoboken, NJ: John Wiley & Sons, Inc. p. 402-404.
14. Gribik, A., D.P. Guillen, and D. Ginosar, *Kinetic Modeling of a Fischer-Tropsch Reaction over a Cobalt Catalyst in a Slurry Bubble Column Reactor for Incorporation into a Computational Multiphase Fluid Dynamics Model*, in *International Pittsburgh Coal Conference 2008*. 2008, September 29 – October 2, 2008: Pittsburgh, PA.
15. Steynberg, A.P., and Dry, M.E., *Fischer-Tropsch Technology*. Studies in Surface Science and Catalysis, ed. G. Centi. Vol. 152. 2006: Elsevier.

APPENDIX
Values for regression coefficients in property equations

Table A1. Values for regression coefficients in liquid hydrocarbon property equations.

	ξ_1	ξ_2	ξ_3	ξ_4	ξ_5	ξ_6
MW	-5.26249E-08	2.68795E-12	-1.23341E-05	-9.53522E+01	1.03320E+00	-1.84674E-04
ρ	-7.07429E-10	1.30075E-12	-2.36017E-05	5.96444E+02	6.08341E-01	-9.56955E-04
μ	1.79025E-13	9.57890E-18	-2.03926E-10	1.57893E-03	-2.75838E-06	1.43360E-09
c_p	-2.31585E-04	7.55333E-09	8.51037E-03	-4.86779E+05	2.56158E+03	1.04205E+00
k	-5.64169E-14	2.66274E-16	-3.37194E-09	1.93724E-01	-1.92020E-04	9.18030E-08
Pr	1.71935E-09	1.99551E-13	-3.30858E-06	1.73954E+01	-8.59123E-03	-7.43486E-08
σ	5.96243E-13	1.25675E-17	-6.16461E-10	4.89329E-02	-7.90545E-05	2.40673E-08

Table A2. Values for regression coefficients in carbon dioxide property equations.

	ξ_1	ξ_2	ξ_3	ξ_4	ξ_5	ξ_6
ρ	-1.25390E-08	-2.28081E-14	1.30890E-05	2.00088E+01	-7.73788E-02	7.38009E-05
μ	-2.35447E-16	2.64499E-21	2.09568E-13	3.93160E-06	5.15621E-08	-1.56605E-11
c_p	-7.30591E-07	-2.15127E-12	5.48923E-04	3.11178E+04	-1.02158E+01	1.52000E-02
k	2.10647E-24	-1.33959E-19	7.85074E-13	3.11252E-03	7.96693E-05	-1.90837E-08
Pr	-2.93158E-11	4.41590E-17	2.17002E-08	8.64163E-01	-5.57856E-04	5.35027E-07

Table A3. Values for regression coefficients in hydrogen property equations.

	ξ_1	ξ_2	ξ_3	ξ_4	ξ_5	ξ_6
ρ	-8.75910E-10	-1.39898E-15	9.27675E-07	1.37977E+00	-5.29761E-03	5.01847E-06
μ	-2.48452E-17	1.74648E-22	2.35718E-14	2.71031E-06	2.25144E-08	-5.09891E-12
c_p	-8.62701E-08	-1.61542E-13	6.07591E-05	2.71274E+04	5.45923E+00	-2.65814E-03
k	1.09099E-23	-6.93408E-19	4.06375E-12	3.58612E-02	5.10847E-04	-1.01628E-07
Pr	-4.31587E-12	9.88441E-18	3.17359E-09	7.38622E-01	-1.38315E-04	8.74823E-08

Table A4. Values for regression coefficients in equations for CO and H_2 diffusion coefficients.

$D_{L,s}$	ξ_1	ξ_2	ξ_3	ξ_4	ξ_5	ξ_6
CO	1.18599E-17	-7.99993E-23	-3.27266E-15	2.47081E-08	-1.34701E-10	2.21670E-13
H_2	1.04809E-17	-9.47682E-23	-2.69480E-15	2.16567E-08	-1.28508E-10	2.26763E-13

Table A5. Values for regression coefficients in equation for Henry's law constants.

H_s	ξ_1	ξ_2	ξ_3	ξ_4	ξ_5	ξ_6
CO	4.68681E-04	7.15978E-08	-1.23962E+00	-1.90891E+07	1.45163E+05	-1.22350E+02
H_2	2.61567E-03	1.00931E-07	-2.66928E+00	3.02048E+07	4.36191E+04	-6.82025E+01

Table A6. Values for regression coefficients in equation for molecular weight of hydrocarbon product mixture.

HC	ξ_1	ξ_2	ξ_3	ξ_4	ξ_5	ξ_6
ε	1.43991E-11	2.00076E-16	-1.17690E-08	8.78877E-01	2.81191E-04	-1.46253E-07
MW_l	-5.26249E-08	2.68795E-12	-1.23341E-05	-9.53522E+01	1.03320E+00	-1.84674E-04
MW_v	-9.81403E-10	6.38883E-14	-9.77897E-08	3.14426E+01	-5.14268E-02	8.03856E-05

Table A7. Values for regression coefficients in equation for water partial pressure.

H_2O	ξ_7	ξ_8	ξ_9	ξ_{10}
P	1.40289E+00	-1.74277E+03	7.38805E+05	-1.06411E+08

Table A8. Values for regression coefficients in gaseous hydrocarbon property equations.

	ξ_1	ξ_2	ξ_3	ξ_4	ξ_5	ξ_6
ρ	-6.93966E-09	1.72886E-14	9.51117E-06	2.35494E+01	-9.39044E-02	9.33258E-05
μ	-1.59834E-16	-2.70601E-22	2.69670E-13	8.32169E-07	3.68418E-08	-1.40560E-11
c_p	-5.38051E-06	1.62315E-10	1.85377E-03	6.46160E+04	-1.42580E+02	3.03757E-01
k	1.04817E-12	-5.55914E-17	-1.56222E-11	-1.98474E-02	1.63646E-04	-2.20302E-08
Pr	-6.46457E-11	5.95938E-16	4.40271E-08	8.55932E-01	-5.45348E-04	6.49952E-07

Table A9. Values for regression coefficients in liquid water property equations.

	ξ_1	ξ_2	ξ_3	ξ_4	ξ_5	ξ_6
ρ	1.07411E-23	2.40265E-26	-1.45361E-19	1.09401E+03	4.46546E-02	-1.39892E-03
μ	-1.31567E-28	1.76460E-32	-4.36713E-26	1.76856E-03	-6.19582E-06	5.71432E-09
c_p	-2.10917E-06	9.57962E-13	8.17283E-04	2.14966E+05	-6.91089E+02	9.14277E-01
k	-3.99546E-26	6.42966E-30	-1.85723E-23	-2.55743E-01	4.56380E-03	-5.52945E-06
Pr	-1.28882E-11	9.73843E-18	4.36054E-09	1.28135E+01	-4.68802E-02	4.58569E-05
σ	-1.60679E-26	1.76160E-30	-2.88485E-24	8.14066E-02	-1.71636E-04	6.72944E-08

Table A10. Values for regression coefficients in water vapor property equations.

	ξ_1	ξ_2	ξ_3	ξ_4	ξ_5	ξ_6
ρ	-1.31582E-08	1.61028E-13	1.11162E-05	1.89252E+01	-7.66428E-02	7.65644E-05
μ	-3.66624E-16	6.49154E-21	2.98575E-13	-1.15802E-06	3.44470E-08	5.30844E-12
c_p	-1.20110E-05	1.62851E-10	7.59538E-03	5.60600E+04	-9.42386E+01	1.04107E-01
k	-3.83553E-27	5.74015E-30	-3.19590E-23	-1.09893E-03	4.90209E-05	5.06316E-08
Pr	-3.79074E-10	4.96761E-15	2.38647E-07	1.88419E+00	-3.57598E-03	3.35923E-06